Title

Recyclable Zinc Ion Structural Supercapacitor Enabled by Porous Vitrimer

Journal

ACS Energy Letters

Authors

Koripally, Nandu

Yao, Lulu

Chambers, Robert

et al.

Publication Date

2026-08-11

DOI

10.1021/acsenergylett.6c01274

ACS Energy LETTERS

http://pubs.acs.org/journal/aelccp

Letter

Recyclable Zinc Ion Structural Supercapacitor Enabled by Porous Vitrimer

Nandu Koripally, Lulu Yao, Robert Chambers, Shengqiang Cai, and Tse Nga Ng*

Cite This: https://doi.org/10.1021/acsenergylett.6c01274

Read Online

ACCESS | Metrics & More | Article Recommendations | Supporting Information

ABSTRACT: Structural electrochemical cells combine load-bearing and energy storage functions to meet growing energy demands in portable systems. However, these integrated composites are difficult to disassemble at the end of life. To attain sustainability, this work engineers vitrimers to create a solid-state electrolyte that delivers mechanical strength, high ionic conductivity, and recyclability for structural energy storage devices. The structural zinc ion supercapacitors achieve a high flexural modulus of 13.9 GPa and a specific energy of 3.57 Wh kg^{-1} at a power density of 18 W kg^{-1}. Integrated into a glider's wings, the multifunctional device powers the onboard motor to extend the flight distance. The composite structure is recyclable through a room-temperature reaction, enabling recovery and reuse of the carbon-fiber cathode. The reclaimed materials are remade into new cells to further extend material lifetime, sustaining over 172,000 redox cycles and demonstrating a promising route towards circular, durable energy storage structures.

Metal ion supercapacitors are electrochemical energy storage systems that store charge through redox reactions at the metal anode and electrostatic ion adsorption at the cathode. Through these surface mechanisms, they show fast kinetics to deliver high power density. However, their low energy density is a constraint limiting their application space. One way to improve energy density is to use a multifunctional energy storage structure, which combines energy storage and load-bearing functions into a single device.[1−6] By leveraging structural volume to increase energy storage capacity, these devices reduce overall mass and weight and extend the operational time of portable electronics and electric vehicles.

However, such an integrated design poses additional challenges to address competing requirements between electrochemical and mechanical properties. The electrodes and electrolytes need structural reinforcement. One crucial link for simultaneously improving structural and electrochemical functions lies in the design of the solid-state electrolyte (SSE), to connect electrodes with high ionic conductivity and concurrently form a composite with high mechanical strength. Most prior works demonstrate mixing thermoset resins with electrolyte salts, but they were limited by poor ionic conductivity due to slow diffusion in the resin, and the salts disrupted cross-linking and degraded mechanical moduli. [1−4,7] To address this challenge with structural SSE, this work explores using dynamic covalent adaptive networks of vitrimers[8−10] to enable high-performance, recyclable structural supercapacitors.

Vitrimers have been gaining traction as reprocessable alternatives to permanent thermoset binders, on par in mechanical strength but with reversible cross-links through heat-activated dynamic bond exchange.[11,12] While previous reports demonstrated vitrimers as the enabling component in recyclable composites for mechanical structures,[13] electronic printed circuit boards,[14] and lithium batteries,[15] those studies mostly isolated mechanical and electrochemical functions into separate domains, for instance, either as reformable mechanical supports[16−18] or a repairable solid-state electrolyte in electrochemical energy storage.[19,20] This work combines mechanical and electrochemical functions and uses vitrimers as thin, porous interfacial coatings that bind mechanically strong components to achieve composite strength. The electrochemical and mechanical properties of the vitrimer-modified electrolyte layers and full cells are compared with those fabricated with conventional epoxy and shown to offer superior performance. The architecture of fiber films coated with thin, porous vitrimer binder overcomes the trade-off in prior works between ionic transport and structural strength, by allowing porosity for high ionic conductivity while providing strong fiber-reinforced mechanical support.

The structural energy storage devices developed in this work are zinc ion supercapacitors, with zinc chemistry selected because of its environmental stability, safety, and high volumetric capacity compared to lithium.[21−24] A zinc metal anode is paired with an activated-carbon cathode, a hybrid combination of redox and capacitive mechanisms [25−30] to enhance energy

Received: April 23, 2026
Revised: July 8, 2026
Accepted: July 14, 2026

density while maintaining long cycle life, which is essential as these devices are integrated as mechanical supports that are not frequently replaced. High-strength laminates with durable energy storage are attractive to aviation and maritime industries where structural composites are already prevalent.[31,32] As a proof-of-concept demonstration, this work integrates multiple structural supercapacitors, scaled up to a total area of 42.85 cm^2, into the wings of a model plane to power the propeller motor and extend the flight distance.

Furthermore, with the global problem of sustainability and electronic waste, it is important to consider materials reuse and recyclability. The devices should allow for reversible debonding at the end of life,[14,33−35] to facilitate cost-effective separation and recovery of high-valued components, including critical elements and carbon fibers (CF). New CF fabrication requires 195−595 MJ kg^{-1} of energy, whereas CF recovery through conventional milling or high-temperature chemical treatments reduces the energy use to 38 MJ kg^{-1}, but the recovered CF may be weaker due to processing damage or contamination.[32] This work reports the mild, room-temperature recovery afforded by vitrimers, further lowering energy costs while maintaining performance. The structural supercapacitors are disassembled by simple chemical solvolysis that uncrosslinks the disulfide vitrimer network at room-temperature quickly within 30 min of submersion. High-value carbon-fiber (CF) substrates used in the cathodes are recycled two times to evaluate the feasibility of recovery and reuse. Although some material loss occurs in the recycling process, the mechanical strength of the recovered CF is preserved, as evident by tensile stress characterization. The recycled structural supercapacitors retain competitive specific power, energy, and cycling stability, underscoring the potential of these sustainable devices for minimizing electronic waste while addressing the energy storage demands of our increasingly electrified world.

Properties of Vitrimer Structural Electrolytes

The function of electrolytes is to facilitate efficient ionic conduction for charge balance while keeping electrodes electrically insulated to prevent an internal short circuit. To ensure good electrical separation, electrochemical cells often have a separator film placed between electrodes. With solid-state electrolytes, the solid films may combine physical separation and ionic transport functions. In our work here, we fabricated solid-state electrolytes from commercially available separator films modified with various binder coatings and evaluated their ionic conductivity and mechanical characteristics. This approach allows easy tuning of coating properties while maintaining film integrity for process handling and heat lamination to bond all cell layers together for structural strength. The modified separator films were infused with 7.5 M $ZnCl_2$ aqueous solution, thereby incorporating high salt concentration to complete the structural solid-state electrolyte. This water-in-salt composition was chosen for its wide potential window, high-power compatibility, broad temperature range, and nonflammability,[36,37] a safer and more environmentally friendly alternative to organic solvents.

As shown in Figure 1, the coating materials for the structural electrolyte were bisphenol A diglycidyl ether (DGEBA) resin[38] and 2-aminophenyl disulfide (2-AFD) cross-linker[39−41] to form the vitrimer. If the formulation included water-soluble polyethylene glycol (PEG),[42,43] after cross-linker curing, the PEG was dissolved away in deionized water to leave behind a porous vitrimer. The coating materials were mixed together at 90 °C and dropcast onto commercial polypropylene separator films consisting of hydrophilic woven fiber networks and cured at 150 °C for 4 h. The separator serves as a structural frame for the vitrimer and a physical spacer to consistently control the thickness and uniformity and to prevent collapse of the porous film. The materials and processing procedures are provided in detail in the Methods Section in the Supporting Information. The chemical structures of the DGEBA, 2-AFD, PEG, polypropylene, vitrimer, and porous vitrimer were characterized by Fourier transform infrared spectroscopy (FTIR) in Figure S1. In the differential scanning calorimetry (DSC) analysis in Figure S2a, the glass transition, T_g, of both vitrimers was 125 °C. The peaks are enthalpy relaxation peaks indicating structural relaxation of a glassy material, previously reported in DGEBA-based vitrimers near the glass transition temperature.[44,45] Figure S2b shows the thermogravimetric analysis (TGA) of the polypropylene separator, vitrimer, and porous vitrimer films. The separator degrades at 440 °C, the vitrimer

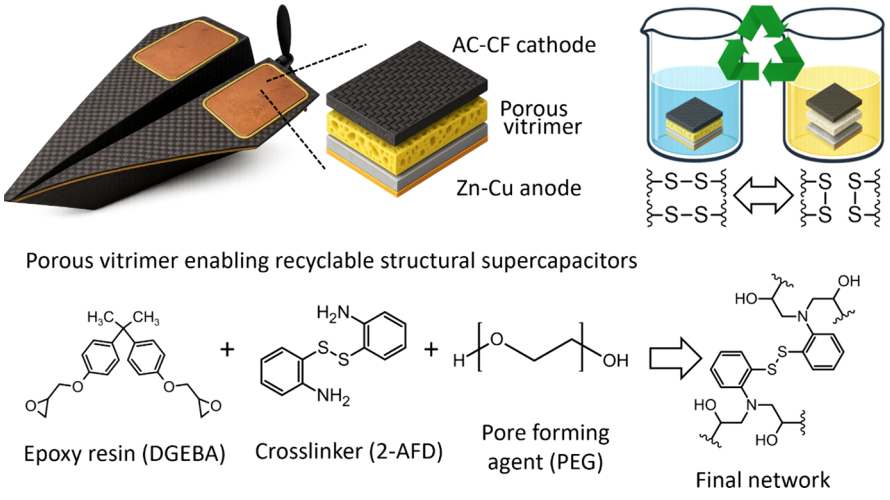

Figure 1. Schematics of recyclable structural supercapacitors. The porous vitrimer composed of DGEBA, 2-AFD, and PEG contains reformable disulfide bonds, which bind the electrodes and separator layers together to form structural zinc ion supercapacitors. The cross-linking is reversible by chemical solvolysis at room temperature to recover and reuse electrode materials such as carbon fibers.

https://doi.org/10.1021/acsenergylett.6c01274
ACS Energy Lett. XXXX, XXX, XXX−XXX

degrades at 230 °C, and the porous vitrimer at 227 °C. All sample dimensions are specified in Table S1.

The ionic conductivity of structural electrolytes was tuned by applying vitrimer mixtures at different loadings onto the separator substrates, and the amount of pore-forming agent PEG in the vitrimer was also varied, as shown in Figure 2a. With a 7.5 M $ZnCl_2$ electrolyte, the ionic conductivity of these electrolyte films was calculated from the equivalent series resistance measured in electrochemical impedance spectroscopy (EIS). The samples with the highest ionic conductivity were made from loading at 4 mg cm^{-2}, with a PEG content of 33% and 50% by weight in the vitrimer mixture, yielding 4.55 ± 0.4 and 4.08 ± 0.4 mS cm^{-1}, respectively. These conductivity values exceed those of previously reported structural electrolytes[3,46,47] by at least 10-fold, owing to PEG dissolution that restored separator porosity and created free volume in the vitrimer binder to enhance ionic percolation beyond what was achievable with polymer additives or ionic-liquid phase separation methods.[3,43,46]

Minimizing vitrimer loading on separator substrates while maintaining a uniform coating was essential for maximizing ionic conductivity. Here, our minimum loading was at 4 mg cm^{-2}. A broad processing window was observed for PEG contents, in that between 33 and 50% PEG, high ionic conductivity was consistently achieved, allowing wide tolerance to ensure repeatability. For processing, the 50% PEG formulation was less viscous and easier to control deposition than the 30% mixture. Increasing PEG content beyond 50% introduced excessive voids, resulting in weak vitrimer structures that partially collapsed after PEG dissolution. For formulations with >60% PEG, the vitrimer matrix never properly cross-linked.

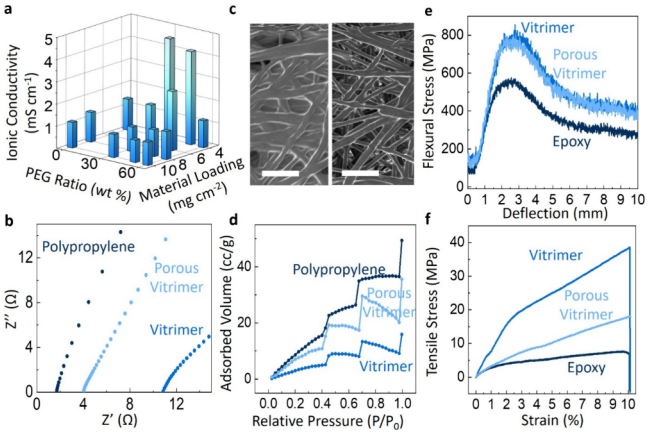

Figure 2. Characterization of structural electrolyte films. Films had been infused with 7.5 M $ZnCl_2$ aqueous solution to incorporate salts for ionic transport. (a) Ionic conductivity as a function of vitrimer composition and material loading onto the separator substrate. The weight ratio of DGEBA:2-AFD blend was held constant at 2:3 in this dataset, while the same blend was adjusted with PEG by weight percentage. (b) Electrochemical impedance of a polypropylene separator as purchased (dark blue), following vitrimer coating before PEG dissolution (medium blue), and after PEG removal (light blue). Scale bar: 100 μm. (c) SEM images of the vitrimer-coated separator before (left) and after (right) dissolving PEG. (d) BET analysis to estimate surface area by the Rouquerol criteria and total pore volume obtained by Gurvich's rule, explained in the Experimental Methods section. (e) Flexural stress versus deflection distance measured on separators coated with epoxy, vitrimer, or porous vitrimer. (f) Tensile stress versus applied strain on separators coated with epoxy, vitrimer, or porous vitrimer.

Overall, the vitrimer formulation used for all subsequent experiments was DGEBA:2-AFD:PEG at a 2:3:5 ratio by weight at 4 mg cm^{-2} loading after PEG dissolution, which contributed an additional coating thickness of ∼30 ± 5 μm on the 130 μm polypropylene separator. Figure 2b compares the EIS characteristics of the separator substrate and vitrimer-coated separators before and after PEG removal. In a 7.5 M $ZnCl_2$ electrolyte, the separator on its own showed an ionic resistance of 1.7 ± 0.1 Ω. The solid vitrimer coating increased the resistance 10-fold to 10.9 ± 0.2 Ω, but following PEG dissolution, the porous vitrimer lowered the resistance to 4.0 ± 0.2 Ω. The recovery of porosity was evident in the scanning electron microscopy (SEM) image in Figure 2c and the cross-sectional images in Figure S3, where the separator fibers were distinct and separated by open volume. The film porosity was estimated from Brunauer–Emmett–Teller (BET) analysis, as shown in Figure 2d. Abrupt jumps in the data were attributed to multilayer surface adsorption.[48] At standard measurement temperature of 77 K and pressure of 1 atm, the surface area of the pristine separator was 55 ± 6 m^2 g^{-1}, with a total pore volume of 0.076 cc g^{-1}. The vitrimer coating reduced the surface area to 18 ± 2 m^2 g^{-1}, with a total pore volume of 0.024 cc g^{-1}. Dissolving the PEG in the vitrimer coating made it more porous, as indicated by a surface area of 36 ± 2 m^2 g^{-1}, with a total pore volume of 0.055 cc g^{-1}.

The mechanical properties of the modified separators were assessed through three-point flexural bend tests and uniaxial tensile tests. One sample was coated with a conventional epoxy cured using permanent aliphatic amine cross-linkers (chemical structures of the cross-linking hardeners in Figure S4). This epoxy has been used previously in high-performance structural supercapacitors[3] and serves as a benchmark for comparison with the reversible disulfide vitrimer coatings. The flexural test results in Figure 2e show that the vitrimer coatings withstood greater flexural stress than the conventional epoxy. The maximum flexural strength reached 770 ± 23 MPa for the nonporous vitrimer coating, 755 ± 21 MPa for the porous vitrimer, and 540 ± 15 MPa for the conventional epoxy. The lower flexural strength of conventional epoxy may be attributed to the longer aliphatic chains in its cross-linkers relative to the compact molecular structure of aminophenyl disulfide, forming a more rigid vitrimer network.

Interestingly, the vitrimer coatings displayed similar flexural strengths before and after PEG dissolution, with the porous vitrimer showing only a slight decrease that remained within one standard deviation of the nonporous sample. The laterally continuous disulfide cross-linked network provided the primary flexural support, rendering the microscale pores negligible to flexural strength. In contrast, the tensile strength was impacted by porosity. In Figure 2f, the maximum tensile stress was highest for the separator coated with nonporous vitrimer at 43 ± 1 MPa, followed by the porous vitrimer at 22 ± 1 MPa, and the conventional epoxy at 11 ± 1MPa. Tensile strength was reduced by half in the porous vitrimer compared to the nonporous film, consistent with the 50% PEG formulation, as PEG removal left half of the volume open and a proportional decrease in tensile load support. All samples broke apart at ∼10% tensile strain, reflecting the failure strain of the polypropylene separator substrate. While separator materials can be changed easily, in the next step of integrating full structural cells, carbon-fiber electrodes would be incorporated to provide the primary tensile reinforcement, and the separator strength

https://doi.org/10.1021/acsenergylett.6c01274
ACS Energy Lett. XXXX, XXX, XXX–XXX

would be secondary. For the structural electrolyte, our approach to coat porous vitrimers onto separator substrates afforded a solid-state electrolyte that combined state-of-the-art ionic conductivity, superior mechanical strength better than conventional epoxy, and reversible covalent bonding capability, ready for binding together the components in structural supercapacitors.

Performance of Structural Zn Ion Supercapacitors

Rechargeable electrochemical cells using zinc metal anodes are under intense development because of their advantages in low cost, intrinsic safety, and high divalent capacity.[5,21,49] This work focused specifically on supercapacitors based on zinc anodes and activated-carbon (AC) cathodes, which are better suited to achieve long lifetimes required in structural energy storage applications. In contrast to battery-type cathodes, AC is capacitive and supports fast kinetics, enabling high current densities for high-power charging/discharging,[27,50] which also mitigates zinc dendritic growth and short circuits.[28−30]

The electrode fabrication process is based on our prior work[30] but adapted for multifunctional structures as detailed in Figure S5. For the cathode, AC was coated onto CF substrates, which served as the current collector as well as mechanical reinforcement in the structural composite. The AC on the CF cathode was treated via a room-temperature Cl_2-gas evolution process that increased AC porosity and thereby enhanced capacitance as reported in ref 30. For the anode, Zn was electroplated onto copper foil current collectors with sputtered copper nanoparticles to promote planar deposition in Zn (002) orientation and mitigate Zn dendrite shorts.[30,51] The capacity ratio between the negative and positive electrodes (n/p) should ideally be balanced to n/p = 1 for maximum utilization of all active materials. However, in practice, current implementations for Zn metal cells mostly use n/p ratios between 10 to 2.5 to extend rechargeable cycle life.[51] The excess Zn capacity compensated for losses from nonuniform replating and disconnections. Although an n/p ratio of >1 would reduce the overall cell-specific capacity, this work chose an n/p ratio of 5 for all fabricated devices to balance capacity and cycling stability, accommodating for the decrease in Zn active area under structural bonding.

The three components—AC on CF (cathode, 230 μm thick), porous vitrimer separator with 7.5 M $ZnCl_2$ (structural electrolyte, 200 μm thick), and Zn on Cu foil (anode, 25 μm thick)—were heat laminated together at 130 °C for 30 s, during which disulfide bonds on the separator surface were reactivated to cross-link with the electrodes, forming a strong laminate with electrochemical storage capability across a 2 V potential window. In comparison with conventional epoxy bonding, the laminate bonded via porous vitrimer was stiffer and supported a 50 g weight without bending, whereas the epoxy-bonded sample was significantly bent under a 20 g weight, as seen in Figure 3a, also consistent with mechanical test results in Figure 2e. Conventional epoxy requires all the components to be cured all at once slowly (>12 h at 25 °C), and the epoxy may reflow and block pores in AC. The rapid 30 s vitrimer lamination preserved porosity in the separator membrane and achieved robust mechanical strength in a thin ∼450 ± 20 μm structure. Figure S6 shows that the porous vitrimer network is preserved after heat laminating. A cross-sectional SEM view of the structural supercapacitor in Figure 3b and Figure S7 shows distinct layers after lamination.

To serve as a multifunctional structure simultaneously providing energy storage and mechanical support, the structural

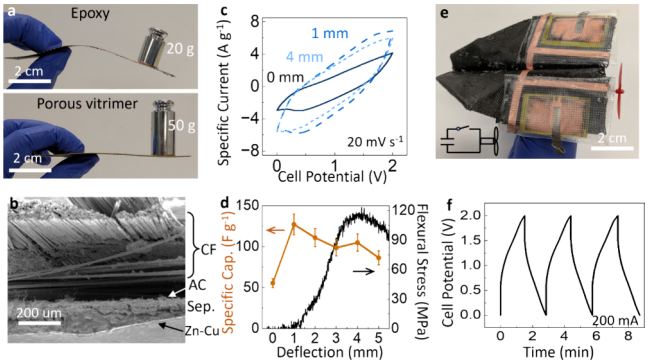

Figure 3. Characterization of structural supercapacitors. (a) Photographs showing the deflection of full cells with different binders. (b) Cross-sectional SEM image of the structural supercapacitor. (c) Cyclic voltammetry measured at a scan rate of 20 mV s^{-1}, as the structural supercapacitor was subjected to increasing flexural deflection from 0 to 4 mm. (d) Specific capacitance and flexural stress as a function of deflection distance. The specific current and capacitance were calculated using the weight of active materials (AC & Zn = 4.56 mg). (e) A photograph and a circuit schematic of a model plane, in which four structural supercapacitors connected in parallel were integrated onto the top and bottom surfaces of the wing sections. (f) Charge−discharge voltage profiles versus time, at a constant current of 200 mA (equivalent to 4.67 mA cm^{-2} and 0.204 A g^{-1}) for the integrated supercapacitors on the model plane.

supercapacitor was characterized by cyclic voltammetry (CV) under varying flexural deflection applied at the midpoint of a 1 × 10 cm^2 sample area. As shown in Figure 3c, upon bending the initially flat device to a 1 mm deflection, the current−voltage curve increased, indicating improved electrical contact between active layers under the bending pressure. The corresponding specific capacitance in Figure 3d, calculated from the CV using the total mass of active materials (AC and Zn), rose from 55 F g^{-1} in the flat state to 126 F g^{-1} under a 1 mm deflection. However, with further deflection between 2 and 4 mm, the carbon-fiber weave began to splinter, and the capacitance gradually decreased to 104 F g^{-1} at 4 mm deflection, when the device reached irreversible deformation at a maximum flexural stress of 112 ± 4 MPa. The flexural modulus was 13.9 ± 1.4 GPa. The tensile strength of the structural supercapacitor was reinforced by the CF to reach a maximum tensile stress of 92 ± 0.1 MPa and a tensile modulus of 7.32 ± 1.40 GPa in Figure S8. The tensile stress-strain behavior of the structural supercapacitor reflected the combined response of the CF and separator substrates, such that the CF conferred high tensile strength until its break point at 2% strain, and then the structure continued in tensile creep until 5% strain when the vitrimer separator ruptured.

To demonstrate process scalability and motivated by the use of carbon-fiber laminates in aerial structures such as planes and drones, we fabricated a folded glider with wings incorporating structural supercapacitors to provide mechanical support and energy storage for the propeller motor, as shown in Figure 3e and stepwise in Figure S9. The fabrication process began with the deposition and lamination of supercapacitor materials onto the wing regions, defining four devices connected in parallel that summed to a total active area of 42.85 cm^2, with a loading of 904 mg AC and 78 mg Zn. The loading mass of AC is higher than Zn, while the n/p ratio is still at 5, because of the much

https://doi.org/10.1021/acsenergylett.6c01274
ACS Energy Lett. XXXX, XXX, XXX−XXX

higher capacity of Zn compared to AC (see calculation in eq S2). Conductive copper tape was applied to the CF substrate to improve electrical conductivity across the sheet, and titanium foil tabs were attached to the anode current collectors with epoxy. The aqueous 7.5M $ZnCl_2$ electrolyte was dropcast onto the CF and separator edges and driven by capillary wicking into the laminate, which was then vacuum sealed between polyethylene terephthalate (PET) sheets. The rest of the CF sheet was folded into a glider shape and fixed in place with commercial epoxy. A toggle on/off switch and a motor circuit were soldered to the Cu tape and Ti tab contacts under the plane.

With the four structural supercapacitors connected in parallel, the full device capacitance was 8.09 F (equivalent to 0.188 F cm^{-2} and 8.23 F g^{-1} based on active materials (AC and Zn weight) as measured in Figure 3f when it was cycled between 2 V at a constant current of 200 mA (equivalent to 4.67 A cm^{-2} and 0.204 A g^{-1}; all the specific weights used in calculations are detailed in Supplemental Table S1). With the large area and cells connected in parallel, the device equivalent series resistance was only 1.4 Ω in Supplemental Figure S10. Based on the active materials' weight, the device-specific energy was 2.79 Wh kg^{-1} at a power output of 124 W kg^{-1}. If including the full structural weight, including the active materials, vitrimer electrolyte, and current collector substrates, the specific energy was 1.01 Wh kg^{-1} at a power output of 44.9 W kg^{-1}.

Discharging the structural supercapacitors allowed 2 min 16 s of motor run time after 1.5 min of charging at 200 mA. If the glider was thrown with the motor off, it traveled approximately 244 cm (8 feet) before landing on the ground (Figure S10 and Movies S1 and S2). With the motor powered by the supercapacitors, the travel distance extended to 366 cm (12 feet) with a longer glide assisted by the propeller lift. We note that in our proof-of-concept implementation, the glider design was not optimized in weight distribution with a heavy front end due to CF folds and epoxy. However, the demonstration shows the ability of structural supercapacitors to generate enough power for the propeller to move the glider, in which the supercapacitor was 2.716 g and only 8.7% of the total glider weight (31.21 g), and hence moving 11.5 times its own weight.

Performance of Recycled Supercapacitors

Our structural supercapacitors are recyclable at room temperature by solvent debonding of the vitrimer binder. The vitrimer binder was uncross-linked in a solution of tris(2-carboxylethyl)-phosphine hydrochloride (TCEP-HCl), deionized water, and acetone at a 2:3:5 weight ratio in ambient conditions. As a reducing agent, TCEP-HCl cleaved the disulfide bonds (−S−S−) and reduced them to thiols (−S−H) that uncross-linked the polymer, as illustrated in Figure 4a and Figure S11.[11,12] After 2 min of immersion, the electrodes were detached from the vitrimer separator. After 30 min, the vitrimer coating appeared to be mostly dissolved away from the substrates, with the separator returning to its original white surface before the modification by the yellow vitrimer coating.

Since the CF substrates were the costliest among the cell components, they were the focus of our recovery and reuse tests. The retrieved AC-CF cathode was cleaned in 1 M hydrochloric acid (HCl) for 1 min and reweighed. The cathode mass decreased by 15% and 35% upon the first and second recycle, respectively. The tensile stress-strain characteristics followed a similar pattern, with maximum tensile stress decreasing by 19% and 36%, respectively, as seen in Figure S7. While the

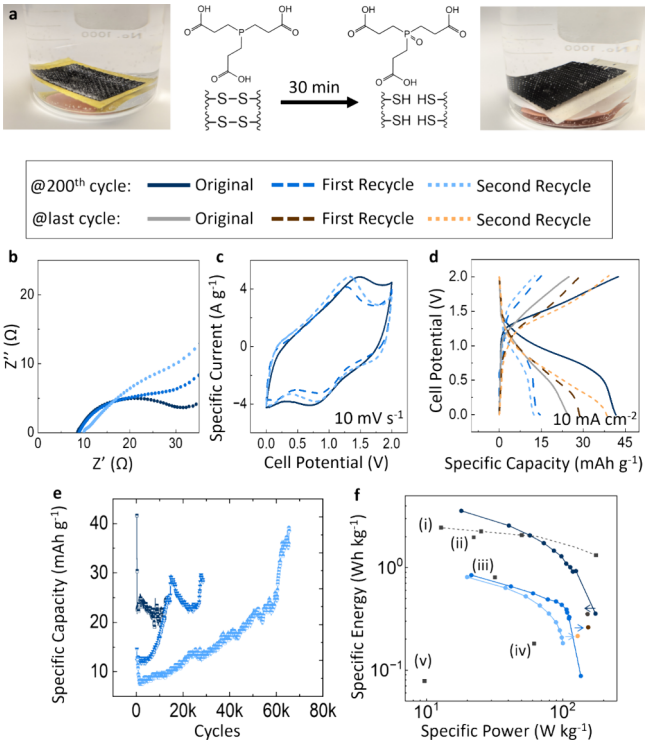

Figure 4. Recycling process and characterization. (a) Structural supercapacitor placed in a TCEP-HCl solution to cleave disulfide bonds at room temperature and separate cell materials for recovery. (b) Electrochemical impedance of the structural supercapacitor in the as-fabricated condition and after refabrication using recycled cathodes. The same color legends apply to panels (b–f). (c) Cyclic voltammetry measured at a scan rate of 10 mV s^{-1} after 40 charge–discharge cycles. (d) Charge–discharge characteristics at a current density of 10 mA cm^{-2} at the 200th cycle (blue) and at the last cycle (gray: 12,600th; brown: 28,500th; orange: 65,500th). (e) Specific capacity, normalized by the AC and Zn active materials weight, versus charge–discharge cycles over 2 V, at a current density of 10 mA cm^{-2}. Measurements on the original device were halted following a short circuit, while those on the recycled devices were stopped due to time constraints. (f) Specific energy versus specific power of structural supercapacitors, normalized to full device weight: (i) QxTh-rGO,[3] (ii) $LiCoO_2$-CF,[52] (iii) CAG-CFRP,[53] (iv) FCF/E-IL-70-CF,[46] and (v) CNT-MnO_2-CF.[47]

carbon fibers stayed intact and were not damaged by the solvent recovery process, the entire cathode strength decreased proportionally to the loss of the AC binder. At the interface between AC and vitimer, there was competing adhesion for AC to either stay with the polyvinylidene fluoride (PVDF) binder or to be bonded with vitrimer. While the TCEP-HCl did not attack PVDF, some AC particles that were merged into the vitrimer electrolyte were washed away during vitrimer dissolution.

The recovered AC-CF cathodes were reused two more times to evaluate the performance of recycled cells. In the following recycling feasibility tests, we reassembled the recycled cathodes with new porous vitrimer electrolytes and freshly electroplated Zn anodes to isolate performance changes due to the cathode being the primary target material for recycling.

In Figure 4b, the original structural supercapacitor made from all new materials showed an equivalent series resistance (ESR) at 8.6 ± 0.1 Ω, and the device ESR increased to 9.0 ± 0.1 and 10 ± 0.1 Ω after the first and second round of cathode recycling, respectively. Correspondingly, Figure 4c shows that

https://doi.org/10.1021/acsenergylett.6c01274
ACS Energy Lett. XXXX, XXX, XXX–XXX

the recycled devices have slightly lower specific current than the original device. The sequential CV measurements in Figure S12 provide more data for explaining this observation. The AC-CF cathode was measured as a free-standing electrode, followed by another measurement after it was bonded by vitrimer as an integrated part of the structural supercapacitor. With all new materials, the current difference between a free-standing and bonded cathode was small. In contrast, after the first recovery, the recycled cathode showed a current drop as a free-standing electrode, and then the current dropped further when it was rebonded.

The first current drop was consistent with the measured weight loss, where part of the AC coating was washed away during vitrimer removal. The second current drop suggests that some active sites in AC might be blocked by residual disulfide cross-linkers that were not completely cleaned out from deep pores in AC. During heat lamination and rebonding, the cross-linker residue may recross-link and thus lower the surface accessibility and cathode capacity. By the second recycling round, the performance loss had stabilized to the level of the first recycling round because the residual cross-linker effect was comparable to that of the first recycling round. The recycled AC coating was not subjected to additional Cl_2 gas activation, and introducing this step in future studies might restore blocked pores. Alternatively, changing the AC binder from PVDF to vitrimer may facilitate separate recovery and regeneration of the AC, independent of the CF substrate recycling.

Calculated based on active materials weight, Figure 4d compares the specific capacities between the original and recycled structural supercapacitors operating in a 2 V potential window and at a constant current density of 10 mA cm^{-2} (equivalent to 10.4, 16.4, and 22.7 A g^{-1}, respectively) in galvanostatic charge−discharge (GCD) measurements. At the 200th GCD cycle, the device showed a specific capacity of 41 mAh g^{-1} or 74 F g^{-1} for the original fabrication, 14 mAh g^{-1} or 25 F g^{-1} for the first recycle, and 12 mAh g^{-1} or 22 F g^{-1} for the second recycle, indicating lower capacities in recycled devices at this point. However, these initially measured capacities were lower-bound values; with continued GCD cycling, the capacities gradually increased, reaching 28 mAh g^{-1} or 50 F g^{-1} at 28,500th GCD cycles for the once-recycled device, and 38 mAh g^{-1} or 68 F g^{-1} at 65,500th GCD cycles for the twice-recycled device.

Interestingly, as seen in Figure 4e, the device performance recovered to the original level with extended GCD cycling. Because the Coulombic efficiency remained consistently around 99.9% throughout all GCD cycles in Figure S13, the gradual increase in the capacity was not attributed to side reactions or charge−discharge imbalance. Instead, it is likely due to improved accessibility of electrochemically active sites as electrolyte salts gradually diffused around blocked AC pores and into the electrodes, assisted by the applied electric field during GCD cycling.

Figure 4e also showcased the long-term cycling stability of the structural supercapacitors. The original device was able to withstand 12,600 GCD cycles before short circuit failure. This cycle life sums to an equivalent of 38 discharge hours. For the recycled devices, they were not tested to the point of short circuit failure. Instead, the GCD cycling was stopped when the measured capacity reached the level of the original device (Figure S13). For the once-recycled sample, it took about 10,000 cycles to recover to a similar capacity as the original, and GCD cycling was continued further to 28,500 cycles, which in total was equivalent to approximately 35 discharge hours. The twice-recycled sample approached the original capacity by 56,500 GCD cycles, and its capacity peaked around 65,500 GCD cycles. The device was cycled further until 131,000 cycles, equivalent to 103 discharge hours, when capacitance decreased from Zn depletion. The initially low capacity of the recycled cathode corresponded to shorter GCD cycle durations, and that is the reason that the cumulative discharge time was not directly proportional to cycle count alone but dependent on both the evolving GCD duration and cycle count. Figure S14 shows another device fabricated and recycled. The same GCD behavior confirms the cathode reactivating after bonding to the vitrimer. Figure S15 also shows the CV data during stability cycling for another device; the fluctuating CV confirms the bonded AC pores becoming more accessible.

From these GCD cycling results, the cumulative capacity was calculated to be 2.1 Ah g^{-1} for the original structural supercapacitor, 3.1 Ah g^{-1} for the once-recycled device, and 14.4 Ah g^{-1} for the twice-recycled device, for a total of 19.6 Ah g^{-1} across the entire lifecycle (Figure S13). These values demonstrate that recycled devices retained cumulative energy storage capacities comparable to their original performance. In addition, the device was cycling in a high-power region at 10 mA cm^{-2}, in contrast to prior works that cycled only at 2−5 mA cm^{-2}. Within the class of zinc metal supercapacitors and batteries shown in Figure S16, our devices provided high specific power on par with cells using liquid[26,54−57] and hydrogel electrolytes,[58,59] while our solid-state electrolyte offered additional mechanical strength and multifunctionality.

Figure 4f compares the specific power and energy of the devices in this work with other structural supercapacitors as detailed in Tables S2 and S3. Our calculations were based on GCD measurements across a wide current density range of 1−20 mA cm^{-2} (equivalent to 1.9−33 A g^{-1}) in Figure S17, normalized by the entire device weight, including active materials, electrolyte, and current collectors. For our devices, at an output power of 18.03 W kg^{-1}, the maximum specific energy was 3.57 Wh kg^{-1}, which exceeded prior reports. Meanwhile, a high-power output of 174.40 W kg^{-1} was achieved, with a corresponding specific energy of 0.35 Wh kg^{-1}. The high-power delivery was enabled by our solid-state electrolytes with high ionic conductivity. While ref 3 as denoted by curve (i) reported a higher specific energy at high-power levels, this work overtook and outperformed in specific energy for operating power below 50 W kg^{-1}. Furthermore, all previously reported structural supercapacitors were not recyclable. Here, the recycled supercapacitors initially exhibited lower-bound performance as indicated by the blue lines. However, with continued GCD cycling, their performance progressively improved and ultimately matched that of devices made from new materials. The slow reactivation of blocked AC pores in recycled cathodes may be accelerated by incorporating additional AC treatment steps between recycles, or separating AC and CF reuse in future studies.

This work has developed recyclable structural supercapacitors that promote a circular lifecycle, demonstrating high-performance multifunctional structures through reusing AC-CF electrodes to reduce cost and waste. Central to this platform is the porous vitrimer binder, which enables solid-state electrolytes with a high ionic conductivity of 4.1 mS cm^{-1}, allowing energy-dense, high-power delivery, along with a strong flexural strength up to 755 MPa to simultaneously provide

https://doi.org/10.1021/acsenergylett.6c01274
ACS Energy Lett. XXXX, XXX, XXX−XXX

load-bearing support and energy storage. While this study focuses on the environmentally stable Zn−AC system, our vitrimer approach is versatile and compatible with other electrochemical electrodes. The reversible disulfide networks bond rapidly under heat lamination and react with specific reducing agents to debond, offering a straightforward process for recovering and recycling laminate components. As a result of circumventing harsh processing, the AC-CF cathode was remarkably durable, operating over 172,000 charge−discharge cycles across its lifecycle from original fabrication through two recycling rounds.

The fully integrated structural supercapacitors, with a maximum specific energy of 3.57 Wh kg^{-1} at an output power of 18.03 W kg^{-1}, were used to power a glider propeller and extend flight distance, showcasing scalability and feasibility to increase energy storage in drones, wireless electronics, and other electric applications where high-power output and lightweight strength are critical. The demonstrated approach is compatible with series and parallel integration to tailor the voltage window and increase capacity, multilayer architectures for increased rigidity, alternative electrochemical chemistries beyond Zn, and can expand recyclability to other components, such as separators and current collectors, in future studies. In summary, the design and processing principles established in this work present a promising pathway for recyclable structural energy storage that addresses growing energy storage demands and advances sustainability through improved recyclability.

■ ASSOCIATED CONTENT

Supporting Information

The Supporting Information is available free of charge at https://pubs.acs.org/doi/10.1021/acsenergylett.6c01274.

Experimental methods; Supplemental Figures: (1) FTIR of vitrimer and reagants, (2) thermal characterization, (3) cross-sectional SEM of nonporous and porous vitrimer, (4) chemical structure of commercial epoxy and hardener, (5) structural supercapacitor fabrication process, (6) cross-sectional SEM of heat-laminated vitrimer, (7) cross-sectional SEM of laminated full cell, (8) tensile data of AC-CF, porous vitrimer, and full cell, (9) prototype plane fabrication, (10) prototype plane characterization, (11) recycling supercapacitor, (12) recovered AC-CF CV, (13) extended stability cycling, (14) additional recycled device, (15) additional device, (16) Ragone plot versus monofunctional Zn ion supercapacitors and batteries, (17) GCD data used for ragone plot; Tables: (1) specific dimensions of devices, (2) multifunctional efficiency of structural supercapacitors, and (3) metrics of structural energy storage cells (DOCX)

Comparison of glider flight distance with and without supercapacitor power assistance (outdoor) (MP4)

Comparison of glider flight distance with and without supercapacitor power assistance (indoor hallway) (MP4)

■ AUTHOR INFORMATION

Corresponding Author

Tse Nga Ng – *Department of Electrical and Computer Engineering, University of California San Diego, La Jolla, California 92093, United States; Materials Science and Engineering Program, University of California San Diego, La Jolla, California 92093, United States;* orcid.org/0000-0001-6967-559X; Email: tnn046@ucsd.edu

Authors

Nandu Koripally – *Department of Electrical and Computer Engineering, University of California San Diego, La Jolla, California 92093, United States*

Lulu Yao – *Materials Science and Engineering Program, University of California San Diego, La Jolla, California 92093, United States*

Robert Chambers – *Department of Mechanical and Aerospace Engineering, University of California San Diego, La Jolla, California 92093, United States;* orcid.org/0000-0001-8475-4501

Shengqiang Cai – *Materials Science and Engineering Program, University of California San Diego, La Jolla, California 92093, United States; Department of Mechanical and Aerospace Engineering, University of California San Diego, La Jolla, California 92093, United States*

Complete contact information is available at: https://pubs.acs.org/doi/10.1021/acsenergylett.6c01274

Notes

The authors declare no competing financial interest.

■ ACKNOWLEDGMENTS

This work was financially supported by the National Defense Science and Engineering Graduate Fellowship for N.K., the Naval Innovation Science Engineering Center, and NSF CNS-2312715. Part of the work was performed at the San Diego Nanotechnology Infrastructure of UCSD, which is supported by NSF ECCS-2025752, and the UC San Diego Materials Research Science and Engineering Center, which is supported by NSF DMR-2011924.

■ REFERENCES

(1) Greenhalgh, E. S.; Nguyen, S.; Asp, L. E.; Bici, A.; Bismarck, A.; Fam, D.; Johansson, M.; Lindbergh, G.; Lutkenhaus, J. L.; Shaffer, M. S. P.; Shirshova, N.; Srinivasan, M.; Xu, J.; Zenkert, D. Characterization and Reporting Protocols for Structural Power Composites: A Perspective. *Adv. Energy Mater.* **2025**, *15* (42), No. e04702.

(2) Chaudhary, R.; Xu, J.; Xia, Z.; Asp, L. E. Unveiling the Multifunctional Carbon Fiber Structural Battery. *Adv. Mater.* **2024**, *36* (48), No. 2409725.

(3) Yao, L.; Zheng, K.; Koripally, N.; Eedugurala, N.; Azoulay, J. D.; Zhang, X.; Ng, T. N. Structural Pseudocapacitors with Reinforced Interfaces to Increase Multifunctional Efficiency. *Sci. Adv.* **2023**, *9*, No. eadh0069.

(4) Zhou, H.; Li, H.; Li, L.; Liu, T.; Chen, G.; Zhu, Y.; Zhou, L.; Huang, H. Structural Composite Energy Storage Devices—a Review. *Mater. Today Energy* **2022**, *24*, No. 100924.

(5) Wang, M.; Vecchio, D.; Wang, C.; Emre, A.; Xiao, X.; Jiang, Z.; Bogdan, P.; Huang, Y.; Kotov, N. A. Biomorphic Structural Batteries for Robotics. *Sci. Robot.* **2020**, *5* (45), No. eaba1912.

(6) Jin, T.; Ma, Y.; Xiong, Z.; Fan, X.; Luo, Y.; Hui, Z.; Chen, X.; Yang, Y. Bioinspired, Tree-Root-Like Interfacial Designs for Structural Batteries with Enhanced Mechanical Properties. *Adv. Energy Mater.* **2021**, *11* (25), No. 2100997.

(7) Yu, W.; Zhao, G.; Wang, Z.; Tang, J.; Wang, S.; Qiang, J.; Cui, Y.; Chen, Y.; Zhang, L.; Deng, L.; Zhao, L.; Wang, Z. A Zinc-Ion Battery Based Machinable Structure Energy Storage Material with a High

Specific Energy and Good Environmental Adaptability. *Nano Energy* **2025**, *142*, No. 111210.
(8) Zheng, J.; Png, Z. M.; Ng, S. H.; Tham, G. X.; Ye, E.; Goh, S. S.; Loh, X. J.; Li, Z. Vitrimers: Current Research Trends and Their Emerging Applications. *Mater. Today* **2021**, *51*, 586−625.
(9) Schenk, V.; Labastie, K.; Destarac, M.; Olivier, P.; Guerre, M. Vitrimer Composites: Current Status and Future Challenges. *Mater. Adv.* **2022**, *3* (22), 8012−8029.
(10) Wang, Z.; Cai, S. Recent Progress in Dynamic Covalent Chemistries for Liquid Crystal Elastomers. *J. Mater. Chem. B* **2020**, *8* (31), 6610−6623.
(11) Martinez-Diaz, D.; Cortés, A.; Jiménez-Suárez, A.; Prolongo, S. G. Hardener Isomerism and Content of Dynamic Disulfide Bond Effect on Chemical Recycling of Epoxy Networks. *ACS Appl. Polym. Mater.* **2022**, *4* (7), 5068−5076.
(12) Mthembu, S. N.; Sharma, A.; Albericio, F.; de la Torre, B. G. Breaking a Couple: Disulfide Reducing Agents. *ChemBioChem* **2020**, *21* (14), 1947−1954.
(13) Taynton, P.; Ni, H.; Zhu, C.; Yu, K.; Loob, S.; Jin, Y.; Qi, H. J.; Zhang, W. Repairable Woven Carbon Fiber Composites with Full Recyclability Enabled by Malleable Polyimine Networks. *Adv. Mater.* **2016**, *28* (15), 2904−2909.
(14) Zhang, Z.; Biswal, A. K.; Nandi, A.; Frost, K.; Smith, J. A.; Nguyen, B. H.; Patel, S.; Vashisth, A.; Iyer, V. Recyclable Vitrimer-Based Printed Circuit Boards for Sustainable Electronics. *Nat. Sustainable* **2024**, *7* (5), 616−627.
(15) Sun, Z.; Wu, J.; Yuan, H.; Lan, J.; Yu, Y.; Zhu, Y.; Yang, X. Self-Healing Polymer Electrolyte for Long-Life and Recyclable Lithium-Metal Batteries. *Mater. Today Energy* **2022**, *24*, No. 100939.
(16) Zhao, S.; Abu-Omar, M. M. Recyclable and Malleable Epoxy Thermoset Bearing Aromatic Imine Bonds. *Macromolecules* **2018**, *51* (23), 9816−9824.
(17) Ruiz De Luzuriaga, A.; Martin, R.; Markaide, N.; Rekondo, A.; Cabañero, G.; Rodríguez, J.; Odriozola, I. Epoxy Resin with Exchangeable Disulfide Crosslinks to Obtain Reprocessable, Repairable and Recyclable Fiber-Reinforced Thermoset Composites. *Mater. Horiz.* **2016**, *3* (3), 241−247.
(18) Yu, K.; Shi, Q.; Dunn, M. L.; Wang, T.; Qi, H. J. Carbon Fiber Reinforced Thermoset Composite with Near 100% Recyclability. *Adv. Funct. Mater.* **2016**, *26* (33), 6098−6106.
(19) Katcharava, Z.; Marinow, A.; Binder, W. H. Vitrimeric Electrolytes - Overview and Perspectives. *Chem. Commun.* **2025**, *61* (16), 3250−3270.
(20) Sun, Z.; Wu, J.; Yuan, H.; Lan, J.; Yu, Y.; Zhu, Y.; Yang, X. Self-Healing Polymer Electrolyte for Long-Life and Recyclable Lithium-Metal Batteries. *Mater. Today Energy* **2022**, *24*, No. 100939.
(21) Lionetto, F.; Arianpouya, N.; Bozzini, B.; Maffezzoli, A.; Nematollahi, M.; Mele, C. Advances in Zinc-Ion Structural Batteries. *J. Energy Storage* **2024**, *84*, No. 110849.
(22) Liu, X.; Han, Q.; Han, J.; Ma, Q.; Liu, C. Carbon Fiber Reinforced Structural Zn-Ion Battery Composites with Enhanced Mechanical Properties and Energy Storage Performance. *Sustainable Energy Fuels* **2022**, *6* (20), 4669−4680. .
(23) Liang, Y.; Dong, H.; Aurbach, D.; Yao, Y. Current Status and Future Directions of Multivalent Metal-Ion Batteries. *Nat. Energy* **2020**, *5* (9), 646−656.
(24) Shin, C.; Lee, E. H.; Eun, H. J.; Jung, J.; Kim, J. H.; Ng, T. N. Protic Stabilization Engenders High Energy Density and Long Cycle Life in Polyaniline−Zinc Supercapacitors. *Small Sci.* **2024**, *4* (11), No. 2400295.
(25) Zhang, B.; Wu, C.; Bao, Y.; Zou, P.; Wang, X.; Yuan, S.; Chen, G.; Chen, C. Aniline Tetramer Conjugated N-Doped Graphene Aerogel Enabling Efficient PH-Universal Aqueous Supercapacitors. *J. Colloid Interface Sci.* **2025**, *677*, 151−160.
(26) Wang, L.; Peng, M.; Chen, J.; Hu, T.; Yuan, K.; Chen, Y. Eliminating the Micropore Confinement Effect of Carbonaceous Electrodes for Promoting Zn-Ion Storage Capability. *Adv. Mater.* **2022**, *34* (39), No. 2203744.
(27) Shin, C.; Yao, L.; Lin, H.; Liu, P.; Ng, T. N. Photothermal Supercapacitors with Gel Polymer Electrolytes for Wide Temperature Range Operation. *ACS Energy Lett.* **2023**, 1911−1918.
(28) Yu, X.; Li, Z.; Wu, X.; Zhang, H.; Zhao, Q.; Liang, H.; Wang, H.; Chao, D.; Wang, F.; Qiao, Y.; Zhou, H.; Sun, S. G. Ten Concerns of Zn Metal Anode for Rechargeable Aqueous Zinc Batteries. *Joule* **2023**, *7* (6), 1145−1175.
(29) Yang, Y.; Yang, H.; Zhu, R.; Zhou, H. High Reversibility at High Current Density: The Zinc Electrodeposition Principle behind the "Trick."*Energy Environ. Sci.* **2023**, *16* (7), 2723−2731.
(30) Yao, L.; Koripally, N.; Shin, C.; Mu, A.; Chen, Z.; Wang, K.; Ng, T. N. Engineering Electro-Crystallization Orientation and Surface Activation in Wide-Temperature Zinc Ion Supercapacitors. *Nat. Commun.* **2025**, *16* (1), No. 3597.
(31) Jones, C. E.; Norman, P. J.; Burt, G. M.; Hill, C.; Allegri, G.; Yon, J. M.; Hamerton, I.; Trask, R. S. A Route to Sustainable Aviation: A Roadmap for the Realization of Aircraft Components with Electrical and Structural Multifunctionality. In *IEEE Trans. Transp. Electrif.* **2021**, *7* (4), 3032−3049.
(32) Lefeuvre, A.; Garnier, S.; Jacquemin, L.; Pillain, B.; Sonnemann, G. Anticipating In-Use Stocks of Carbon Fiber Reinforced Polymers and Related Waste Flows Generated by the Commercial Aeronautical Sector until 2050. *Resour. Conserv. Recycl.* **2017**, *125*, 264−272.
(33) Dong, Y.; Bao, C.; Kim, W. S. Sustainable Additive Manufacturing of Printed Circuit Boards. *Joule* **2018**, *2* (4), 579−582.
(34) Easley, A. D.; Ma, T.; Lutkenhaus, J. L. Imagining Circular beyond Lithium-Ion Batteries. *Joule* **2022**, *6* (8), 1743−1749.
(35) Barnett, P. R.; Hmeidat, N. S.; Zheng, B.; Penumadu, D. Toward a Circular Economy: Zero-Waste Manufacturing of Carbon Fiber-Reinforced Thermoplastic Composites. *npj Mater. Sustainability* **2024**, *2* (1), No. 3.
(36) Zhang, Q.; Ma, Y.; Lu, Y.; Li, L.; Wan, F.; Zhang, K.; Chen, J. Modulating Electrolyte Structure for Ultralow Temperature Aqueous Zinc Batteries. *Nat. Commun.* **2020**, *11* (1), No. 4463.
(37) Yang, C.; Xia, J.; Cui, C.; Pollard, T. P.; Vatamanu, J.; Faraone, A.; Dura, J. A.; Tyagi, M.; Kattan, A.; Thimsen, E.; Xu, J.; Song, W.; Hu, E.; Ji, X.; Hou, S.; Zhang, X.; Ding, M. S.; Hwang, S.; Su, D.; Ren, Y.; Yang, X. Q.; Wang, H.; Borodin, O.; Wang, C. All-Temperature Zinc Batteries with High-Entropy Aqueous Electrolyte. *Nat. Sustainable* **2023**, *6* (3), 325−335.
(38) Jin, F. L.; Li, X.; Park, S. J. Synthesis and Application of Epoxy Resins: A Review. *J. Ind. Eng. Chem.* **2015**, *29*, 1−11.
(39) Azcune, I.; Odriozola, I. Aromatic Disulfide Crosslinks in Polymer Systems: Self-Healing, Reprocessability, Recyclability and More. *Eur. Polym. J.* **2016**, *84*, 147−160.
(40) Memon, H.; Wei, Y.; Zhu, C. Recyclable and Reformable Epoxy Resins Based on Dynamic Covalent Bonds − Present, Past, and Future. *Polym. Test.* **2022**, *105*, No. 107420.
(41) Yang, Y.; Xu, Y.; Ji, Y.; Wei, Y. Functional Epoxy Vitrimers and Composites. *Prog. Mater. Sci.* **2021**, *120*, No. 100710.
(42) Gu, Y.; Guo, R.; Zhou, Y.; Wang, S.; Li, M. Effects of Porogen Content on Curing Process and Performances of Needled Fiber Preform Reinforced Phenolic Aerogel Composite Using Process Simulation and Comprehensive Experiments. *Composites, Part A* **2025**, *194*, No. 108902.
(43) Feng, Q.; Yang, J.; Yu, Y.; Tian, F.; Zhang, B.; Feng, M.; Wang, S. The Ionic Conductivity, Mechanical Performance and Morphology of Two-Phase Structural Electrolytes Based on Polyethylene Glycol, Epoxy Resin and Nano-Silica. *Mater. Sci. Eng.* **2017**, *219*, 37−44.
(44) Yang, S. J.; Chen, T.; Wagner, R. J.; Page, K. A.; Silberstein, M. N. Physical Aging in Epoxy Vitrimers Enhanced by Catalyst-Modified Network Structure. *Polymer* **2026**, *360*, No. 130339.
(45) Kada, I.; Trinh, D.; Touzain, S.; Mallarino, S. Quantification of Physical Aging Using Two MDSC Methods and Its Effect on Initial Properties of Epoxy Films. *J. Non. Cryst. Solids* **2025**, *649*, No. 123335.
(46) Dharmasiri, B.; Stojcevski, F.; Usman, K. A. S.; Alex Qin, S.; Razal, J. M.; Doeven, E. H.; Francis, P. S.; Connell, T. U.; Yin, Y.; Andersson, G. G.; Borkar, A.; Henderson, L. C. Flexible Carbon Fiber

Based Structural Supercapacitor Composites with Solvate Ionic Liquid-Epoxy Solid Electrolyte. *Chem. Eng. J.* **2023**, *455*, No. 140778.
(47) Tynan, B.; Zhou, Y.; Brown, S. A.; Dai, L.; Rider, A. N.; Wang, C. H. Structural Supercapacitor Electrodes for Energy Storage by Electroless Deposition of MnO_2 on Carbon Nanotube Mats. *Compos. Sci. Technol.* **2023**, *238*, No. 110016.
(48) Sing, K. S. W. *International Union of Pure and Applied Chemistry, Physical Chemistry Division, Commission on Colloid and Surface Chemistry Including Catalysis, Subcommittee on Reporting Gas Adsorption Data, Reporting Physisorption Data for Gas/Solid Systems with Special Reference to the Determination of Surface Area and Porosity*; **1982**; Vol. *54*.
(49) Dong, L.; Ma, X.; Li, Y.; Zhao, L.; Liu, W.; Cheng, J.; Xu, C.; Li, B.; Yang, Q. H.; Kang, F. Extremely Safe, High-Rate and Ultralong-Life Zinc-Ion Hybrid Supercapacitors. *Energy Storage Mater.* **2018**, *13*, 96−102.
(50) Yao, L.; Liu, J.; Eedugurala, N.; Mahalingavelar, P.; Adams, D. J.; Wang, K.; Mayer, K. S.; Azoulay, J. D.; Ng, T. N. Ultrafast High-Energy Micro-Supercapacitors Based on Open-Shell Polymer-Graphene Composites. *Cell Rep. Phys. Sci.* **2022**, No. 100792.
(51) Shin, C.; Yao, L.; Jeong, S.-Y.; Ng, T. N. Zinc-Copper Dual-Ion Electrolytes to Suppress Dendritic Growth and Increase Anode Utilization in Zinc Ion Capacitors. *Sci. Adv.* **2024**, *10*, No. eadf9951.
(52) Javaid, A.; Noreen, S. Mechanically Robust Structural Hybrid Supercapacitors with High Energy Density for Electric Vehicle Applications. *J. Energy Storage* **2022**, *55*, No. 105818.
(53) Qi, G.; Nguyen, S.; Anthony, D. B.; Kucernak, A. R. J.; Shaffer, M. S. P.; Greenhalgh, E. S. The Influence of Fabrication Parameters on the Electrochemical Performance of Multifunctional Structural Supercapacitors. *Multifunct. Mater.* **2021**, *4* (3), 034001.
(54) Wang, Z.; Huang, J.; Guo, Z.; Dong, X.; Liu, Y.; Wang, Y.; Xia, Y. A Metal-Organic Framework Host for Highly Reversible Dendrite-Free Zinc Metal Anodes. *Joule* **2019**, *3* (5), 1289−1300.
(55) Wang, F.; Borodin, O.; Gao, T.; Fan, X.; Sun, W.; Han, F.; Faraone, A.; Dura, J. A.; Xu, K.; Wang, C. Highly Reversible Zinc Metal Anode for Aqueous Batteries. *Nat. Mater.* **2018**, *17* (6), 543−549.
(56) Wang, L.; Peng, M.; Chen, J.; Tang, X.; Li, L.; Hu, T.; Yuan, K.; Chen, Y. High Energy and Power Zinc Ion Capacitors: A Dual-Ion Adsorption and Reversible Chemical Adsorption Coupling Mechanism. *ACS Nano* **2022**, *16* (2), 2877−2888.
(57) Chen, P.; Sun, X.; Pietsch, T.; Plietker, B.; Brunner, E.; Ruck, M. Electrolyte for High-Energy- and Power-Density Zinc Batteries and Ion Capacitors. *Adv. Mater.* **2023**, *35* (7), No. 2207131.
(58) Li, L.; Liu, S.; Liu, W.; Ba, D.; Liu, W.; Gui, Q.; Chen, Y.; Hu, Z.; Li, Y.; Liu, J. Electrolyte Concentration Regulation Boosting Zinc Storage Stability of High-Capacity K0.486V2O5 Cathode for Bendable Quasi-Solid-State Zinc Ion Batteries. *Nano-Micro Lett.* **2021**, *13* (1), No. 34.
(59) Cheng, Y.; Jiao, Y.; Wu, P. Manipulating Zn 002 Deposition Plane with Zirconium Ion Crosslinked Hydrogel Electrolyte toward Dendrite Free Zn Metal Anodes. *Energy Environ. Sci.* **2023**, *16* (10), 4561−4571.

https://doi.org/10.1021/acsenergylett.6c01274
ACS Energy Lett. XXXX, XXX, XXX−XXX